Mathematical Biosciences and Engineering

MBE, 20(2): 1856–1881.
DOI: 10.3934/mbe.2023085
Received: 27 August 2022
Revised: 10 October 2022
Accepted: 18 October 2022
Published: 08 November 2022

http://www.aimspress.com/journal/MBE

Research article

Identification and validation of a new pyroptosis-associated lncRNA signature to predict survival outcomes, immunological responses and drug sensitivity in patients with gastric cancer

Jinsong Liu[1,2,†], Yuyang Dai[2,3,†], Yueyao Lu[4,5], Xiuling Liu[1,2], Jianzhong Deng[1,2], Wenbin Lu[1,2,4,5,*] and Qian Liu[1,2,5,*]

[1] Department of Oncology, Wujin Hospital Affiliated with Jiangsu University, Changzhou 213017, China
[2] Changzhou Key Laboratory of Molecular Diagnostics and Precision Cancer Medicine, Changzhou 213017, China
[3] Department of Radiology, Wujin Hospital Affiliated with Jiangsu University, Changzhou 213017, China
[4] Department of Oncology, The Changzhou Clinical School of Nanjing Medical University, Changzhou 213017, China
[5] Department of Oncology, The Wujin Clinical College of Xuzhou Medical University, Changzhou 213017, China

[†] These authors contributed equally to this work.

*** Correspondence:** Email: 14555271@qq.com, lqian9582@163.com.

Abstract: *Background*: Gastric cancer (GC) ranks fifth in prevalence among carcinomas worldwide. Both pyroptosis and long noncoding RNAs (lncRNAs) play crucial roles in the occurrence and development of gastric cancer. Therefore, we aimed to construct a pyroptosis-associated lncRNA model to predict the outcomes of patients with gastric cancer. *Methods*: Pyroptosis-associated lncRNAs were identified through co-expression analysis. Univariate and multivariate Cox regression analyses were performed using the least absolute shrinkage and selection operator (LASSO). Prognostic values were tested through principal component analysis, a predictive nomogram, functional analysis and Kaplan–Meier analysis. Finally, immunotherapy and drug susceptibility predictions and hub lncRNA validation were performed. *Results*: Using the risk model, GC individuals

were classified into two groups: low-risk and high-risk groups. The prognostic signature could distinguish the different risk groups based on principal component analysis. The area under the curve and the conformance index suggested that this risk model was capable of correctly predicting GC patient outcomes. The predicted incidences of the one-, three-, and five-year overall survivals exhibited perfect conformance. Distinct changes in immunological markers were noted between the two risk groups. Finally, greater levels of appropriate chemotherapies were required in the high-risk group. AC005332.1, AC009812.4 and AP000695.1 levels were significantly increased in gastric tumor tissue compared with normal tissue. *Conclusions*: We created a predictive model based on 10 pyroptosis-associated lncRNAs that could accurately predict the outcomes of GC patients and provide a promising treatment option in the future.

Keywords: gastric cancer; pyroptosis-associated genes; lncRNA; survival outcome; immunological response; drug sensitivity

1. Introduction

Gastric cancer (GC) ranks as the fifth most prevalent tumor worldwide [1]. With 768,793 patients dying globally in 2020, GC ranks fourth in terms of death among cancers [2]. The prognostic outcomes of early GC patients have considerably improved with advancements in detection, surgery and radiotherapy. However, the effect of these strategies is limited, with a median survival duration of less than one year and a poor survival rate of five years, for advanced GC patients [3]. Compared with chemotherapy, molecular and immunological therapies have distinct impacts on the treatment of a small number of advanced GC patients [4–6]. However, the deficiency of indicators to predict the early diagnosis of GC necessitates the construction of a novel prognostic and diagnostic risk model.

Pyroptosis, also known as inflammasome-induced programmed cell death, is a new type of cell death (PCD) [7]. Excessive inflammasome activation in pyroptosis is strongly associated with various human diseases and disorders [8]. For example, gasdermin superfamily proteins are the most common pyroptosis inducers; the N-terminal regions of proteins from this family form pores across the cell membrane, thereby leading to the secretion of IL-1β and IL-18 [9]. In addition, the caspase-1-mediated inflammation-associated cell death pathway in pyroptosis involves the AIM2-, NLRP1-, NLRP3-, NLRC4- and pyrin-inflammasomes, and it is known as the most traditional inflammasome pathway [10]. Compared to standard therapies, induction of pyroptosis represents a potential strategy for cancer treatment [11]. Thus, new pyroptosis-associated markers that expand current knowledge of pyroptosis in GC and forecast the prognosis of GC patients are urgently needed.

lncRNAs with over 200 nucleotides [12] are important regulators of gene expression, growth, differentiation, progression and chromatin dynamics [13]. In a growing number of scientific studies, aberrant expression of lncRNAs has been identified as a prognostic marker in a variety of malignancies. For example, AK023391, a lncRNA that promotes gastric cancer, plays a critical role in stimulating the PI3K/Akt signal transduction pathway and has been used as a predictive and therapeutic biomarker in patients with GC [14]. Furthermore, MT1JP, a downregulated lncRNA in GC linked to GC survival, functions as a type of ncRNA to compete with miR-92a-3p and mediates FBXW7 expression to regulate GC progression [15]. Furthermore, EGR1-induced HNF1A-AS1 modulates a variety of pro- and anti-growth regulators to promote the development of GC, thereby serving as a potential

therapeutic target and prognostic biomarker in this disorder [16]. However, only a limited number of investigations on pyroptosis-associated lncRNAs and their involvement in the prognosis of GC patients have been published to date, representing a gap that needs to be filled. Recently, applications of information and computer technology in health care have expanded rapidly [17], such as bioinformatics analysis, deep learning [18], machine learning [19] and Mendelian stochastic studies [20]. Unlike traditional diagnostic and analytical methods, algorithmic analysis has many advantages, including speed, low cost and high accuracy. This study aimed to construct a predictive model through bioinformatics analysis to solve many problems in the diagnosis and treatment of gastric cancer that are currently being encountered in clinical practice.

TCGA (The Cancer Genome Atlas) was used to obtain the expression profiles of 52 pyroptosis-associated genes and 14056 lncRNAs for our investigation. We built a predictive signature to analyze the survival values of GC patients based on 10 pyroptosis-associated lncRNAs. Then, depending on the median cutoff, the predictive model classified GC individuals into two different risk groups. Survival results, risk states and lncRNA expression levels were analyzed using patient data from the training, testing and entire groups. Furthermore, we examined the prognostic capacity of this constructed model, demonstrating that the predictive signature could recognize the differences between the two risk groups. The model was also utilized to examine the tumor immune microenvironment as well as the tumor immunotherapeutic reaction, and significant changes in the expression of immunological biomarkers were noted between the two risk groups. Then, we analyzed and summarized the mutation data, demonstrating that this model exhibited better predictive ability using tumor mutational burden data. Finally, to identify a more efficacious chemotherapy regimen for GC patients, we used a drug susceptibility analysis to compare the IC_{50} values using the GDSC database [21], demonstrating that the appropriate chemotherapy had better effects in the high-risk group. The validation results from the lnCAR database indicated that AC005332.1, AC009812.4 and AP000695.1 levels were significantly increased in gastric tumor tissue compared with normal tissue, and the overall survival of the patients with GC had statistically significant in high and low AP000695.1 group. These results were consistent with the results based on TCGA GC cohort, which showed that AC005332.1, AC009812.4 and AP000695.1 were crucial biomarkers involved in the regulation of GC progression.

In conclusion, we developed a predictive model for GC patients using hub pyroptosis-associated lncRNAs. The effect of pyroptosis-associated lncRNAs on predicting survival and immunological responses was revealed, providing a new method to identify effective diagnostic biomarkers and paving the way for the treatment of GC patients.

2. Materials and methods

2.1. GC patient information

RNA transcriptome sequencing information of 32 normal samples and 375 GC samples, the corresponding clinical information (age, sex, cancer differentiation grade and TNM stage) and the mutation information were abstracted from TCGA (https://portal.gdc.cancer.gov/) [22]. Normalized RNA-seq data were obtained in the fragment per kilobase million (FPKM) format. GC patients without survival data were omitted to reduce statistical bias. TNM (T: tumor; N: node; M: metastasis).

2.2. Identification of lncRNAs associated with pyroptosis

Fifty-two pyroptosis-associated genes were retrieved from prior publications [23–33]. The specific gene names are shown in Supplementary Table 1. The STRING database (https://string-db.org/) was used to explore possible potential interactions between pyroptosis-associated genes, and a protein interaction network was constructed. We hid disconnected nodes and set a minimum required interaction score (high confidence: 0.007) in the network. We also used the TCGA database to obtain the profiles of lncRNAs and pyroptosis-associated genes. A total of 739 pyroptosis-associated lncRNAs were identified based on Pearson's correlation analysis [34]. |Pearson R| > 0.4 and $p < 0.001$ were employed as criteria. The above results were visualized with a Sankey plot using the R packages limma, dplyr, ggalluvial and ggplot2 [35].

2.3. Construction of a predictive signature

The entire TCGA cohort was classified into training and validation cohorts based on a ratio of 1:1. The training cohort was used to establish a pyroptosis-associated lncRNA model, and the entire and testing cohorts were used to verify this risk model. The clinical baseline information of the above two cohorts is presented in Supplementary Table 2. No statistically significant differences in clinical features were noted between the two datasets ($p > 0.05$). We used univariate Cox regression analysis and survival statistics of GC individuals to assess the prognosis of 739 pyroptosis-associated lncRNAs ($p < 0.05$), and forest plots were drawn. Prognosis-associated lncRNAs were identified using LASSO to narrow the number of lncRNAs (using the penalty parameter estimated by 10-fold cross-validation) [36]. We discovered that 20 pyroptosis-associated lncRNAs were strongly associated with the overall survival (OS) of GC patients. Twenty pyroptosis-associated lncRNAs were analyzed using multivariate Cox regression analysis, and a risk model based on 10 pyroptosis-associated lncRNAs was created [37]. The above process was performed using the R packages survival, caret, glmnet, survminer and timeROC. The risk score was computed using the following formula: Risk score = coe (lncRNA1) × exp (lncRNA1) + coe (lncRNA2) × exp (lncRNA2) + … + coe (lncRNAn) × exp (lncRNAn), where coe (lncRNAn) indicates the coefficient of lncRNAs and exp (lncRNAn) indicates the expression of lncRNAs [38]. The median score was calculated to classify the individuals into two groups: a low-risk group and a high-risk group.

2.4. Kaplan–Meier analysis and principal component analysis

Principal component analysis was used to reduce dimensionality, identify models and visualize different-dimensional data from the whole set of genes [39], 52 pyroptosis genes, 10 pyroptosis-associated lncRNAs and the prognostic signature, depending on the expression data of 10 pyroptosis-associated lncRNAs. Principal component analysis was also used to cluster GC patients, and a 3D scatterplot was used to display the distribution of GC patients with the R package scatterplot3D [37]. All samples containing GC patients were divided into low- and high-risk subsets based on the training set's median, which served as a cutoff criterion. To explain the differences in survival outcomes between the two groups, we employed Kaplan–Meier analysis [40]. This approach was performed with the survminer and survival packages in R.

2.5. Evaluating the independence of the pyroptosis-associated lncRNA model

In GC individuals, multivariate and univariate Cox regression analyses were used to determine whether the risk score was an independent factor compared to other clinical features (age, sex, TNM stage and grade) [41]. To analyze the independent prognosis of the pyroptosis-associated lncRNA model, we used the dplyr, survival, rms and pec packages of R to construct the C-index [42]. The survival, survminer and time ROC packages of R were used to construct the ROC curve [43], which examined the independent predictors associated with various clinical features, such as age, sex, clinical phase, TNM stage and risk score. We assessed the relationship between the model and the clinical features using the chi-square test. The sensitivity and specificity of the predictive signature on the one-, three- and five-year OS of GC patients were also assessed.

2.6. Building and validating a predictive nomogram

Various clinical features (age, sex, TNM stage and grade) and risk scores were established to forecast the one-, three- and five-year OS using a predictive nomogram [44]. To demonstrate the consistency between the practical result and the forecast outcome of this risk model, we also constructed calibration curves using the survival, regplot and rms packages of R. The predictive ability of the proposed nomogram models was demonstrated based on the Hosmer-Lemeshow test.

2.7. Functional analysis

Using the R package limma, the differentially expressed genes (DEGs) between the high- and low-risk groups were discovered. The restricted condition was set to $\log_2$ |fold change| > 1 and false discovery rate < 0.05. To determine the biological activities of the DEGs, we used Gene Ontology analysis [45]. Three parts of the GO analysis, biological process (BP), cellular component (CC) and molecular function (MF), were examined. The R packages clusterProfiler, org.Hs.eg.db, enrichplot, ggplot2, ggpubr and dplyr were used in this approach. The p value was calculated to identify the threshold of outcome, and $p < 0.05$ indicated that the functional statement was considerably enriched.

2.8. The roles of pyroptosis-associated lncRNAs in tumor immune microenvironment

To assist the determination of the quantities of immune pathways and tumor-infiltrating immune cells (TIICs) for each sample in various risk groups, a single sample gene-set enrichment analysis (ssGSEA) score was computed. To study and summarize the mutation information from TCGA, we used the R package maftools. The tumor mutational burden (TMB) was calculated depending on tumor mutant genes [37]. To compare the survival outcomes of patients in different TMB groups, we used the survival package in R. The TMB could be utilized to predict the possibility of an immunotherapeutic response in the future. The waterfall diagram demonstrated the relationship between TMB and risk ratings in GC patients.

2.9. Possible drugs targeting pyroptosis-associated lncRNAs

We performed drug analysis to evaluate the response based on the IC_{50} available in the GDSC database for every sample using the R packages limma, ggpubr, pRRophetic and ggplot2 [46] to identify potential drugs targeting the pyroptosis-associated lncRNA signature for treating GC patients. To compare the IC_{50} differences between popular antineoplastic drugs in the high- and low-risk categories, the Wilcoxon signed rank test was employed. We discovered that 12 compounds had substantial differences in predicted IC_{50} in the two groups, and the high-risk group was more susceptible to the above compounds.

2.10. Validation of hub pyroptosis-associated lncRNAs in the lnCAR database

The lnCAR database (https://lncar.renlab.org/) collected and collated differential expression analysis of 52,306 samples and survival analysis of 12,883 samples from 10 tumors (bladder, breast, cervical, colon, esophageal, gastric, liver, lung, ovarian and prostate cancers) from the GEO database [47]. Low-throughput data, such as real-time PCR and northern blot data, were integrated into the lnCAR database as validation datasets. We analyzed the expression levels of hub pyroptosis-associated lncRNAs in GC from the lnCAR database. We also performed survival analysis of hub pyroptosis-associated lncRNAs in GC from the Sento Academic website (https://www.xiantao.love/).

2.11. Statistical analysis

Statistical analyses were performed with R software (version 4.2.0). Clinicopathological characteristics, TMB and drug sensitivity differences between the high- and low-risk groups were analyzed with the Wilcoxon test. The prognostic values were tested by utilizing principal component analysis, a predictive nomogram, functional analysis and Kaplan–Meier analysis. To compare categorical data among various groups, the chi-square test was employed. Here, $p < 0.05$ was considered statistically significant ($^{*}p < 0.05$; $^{**}p < 0.01$; $^{***}p < 0.001$).

3. Results

3.1. Identification of pyroptosis-associated lncRNAs in patients with GC

The flow chart for constructing the risk model and the subsequent analysis is displayed in Figure 1. TCGA was used to extract the matrix information of 52 pyroptosis-associated genes and 14056 lncRNAs. Pyroptosis-associated lncRNAs were defined as lncRNAs that had a sufficient correlation with 52 pyroptosis genes (|Pearson R| > 0.4 and $p < 0.001$). Finally, using the Sankey plot, the co-expression network of pyroptosis-associated lncRNAs was displayed, and 739 pyroptosis-associated lncRNAs were identified as pyroptosis-associated lncRNAs (Figure 2A). In the entire TCGA cohort, links between 52 pyroptosis genes and 10 prognostic pyroptosis-associated lncRNAs were identified (Figure 2B). A protein interaction network of pyroptosis-associated genes was constructed (Figure S1). These prognostic pyroptosis-associated lncRNAs were used for subsequent model construction.

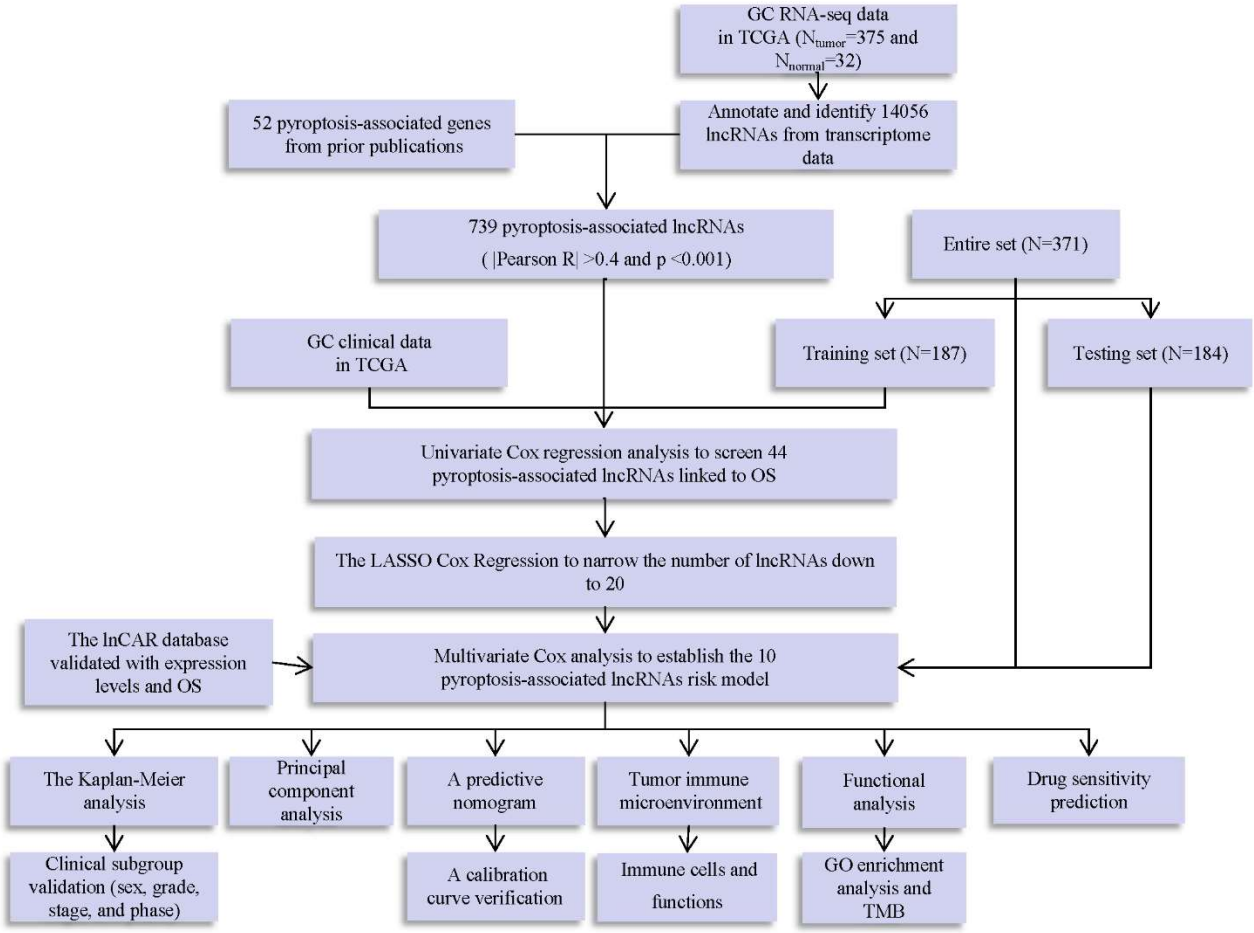

Figure 1. The flowchart of our study. The flowchart depicts the identification and validation of the pyroptosis-associated lncRNA signature. GC: gastric cancer; OS: overall survival.

3.2. Building and validating a risk model based on pyroptosis-associated lncRNAs

In total, 52 pyroptosis-associated lncRNAs associated with OS were screened with univariate Cox regression (Figure 3A). LASSO analysis is a common multiple regression analysis technique. Thus, we used LASSO to narrow the number of lncRNAs to 20 (Figure 3B,C). Furthermore, using multivariate Cox analysis, 10 pyroptosis-associated lncRNAs were identified as prognostic factors that were independently connected with OS and utilized to build a predictive signature to estimate the predictive outcomes in GC patients. The risk model classified GC patients into two different risk categories depending on their median risk score. The scattering of survival outcomes between the two different categories was demonstrated using the entire TCGA cohort (Figure 4A), and survival times were clearly evident when using the entire TCGA cohort (Figure 4B). Distinct expression standards of 10 pyroptosis-associated lncRNAs were represented in the entire TCGA cohort (Figure 4C). Survival analysis revealed that the high-risk group had a lower OS than the low-risk group ($p < 0.001$) in the entire TCGA cohort (Figure 4D).

To test the predictive capacity of the constructed signature, we calculated the risk score for each

individual in the training cohort and testing cohort utilizing the consistent method. The survival results, risk status and lncRNA expression standards of each individual from the training cohort and testing cohort are shown (Figure 5A–C, E–G). The individuals in the high-risk category had a greater risk of dying than those in the low-risk category. Kaplan–Meier analysis revealed that the OS of the high-risk category was obviously lower (Figure 5D,H).

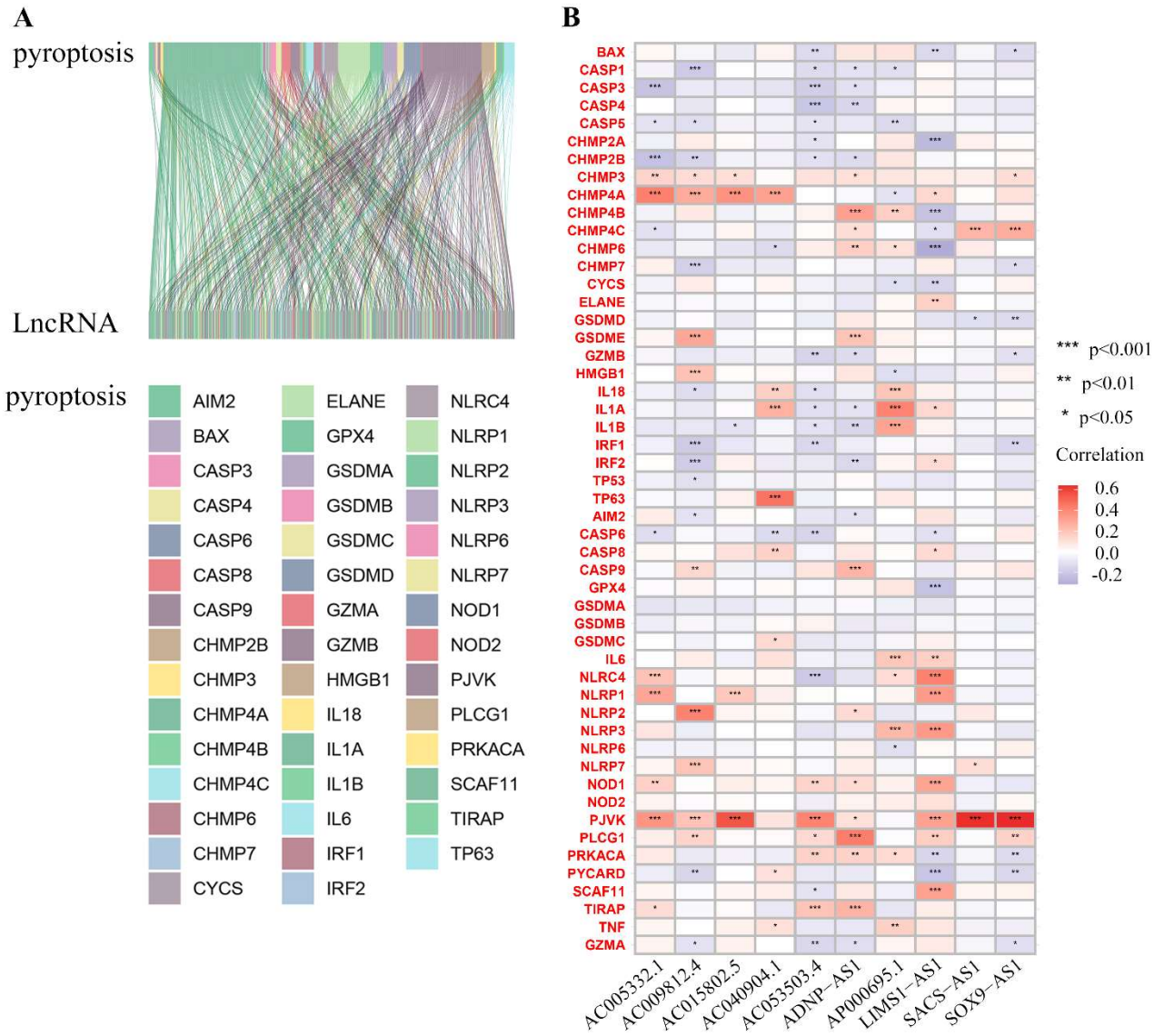

Figure 2. Recognition of pyroptosis-associated lncRNAs in patients with gastric cancer. (A) The Sankey diagram visualizes 52 pyroptosis-associated genes and 739 pyroptosis-associated lncRNAs. Different colors represent the connections between different genes and the corresponding lncRNAs. (B) The connections for 52 pyroptosis-associated genes and 10 prognostic pyroptosis-associated lncRNAs are depicted in the heatmap. Red represents a positive correlation, and blue represents a negative correlation. *$p < 0.05$; **$p < 0.01$; ***$p < 0.001$.

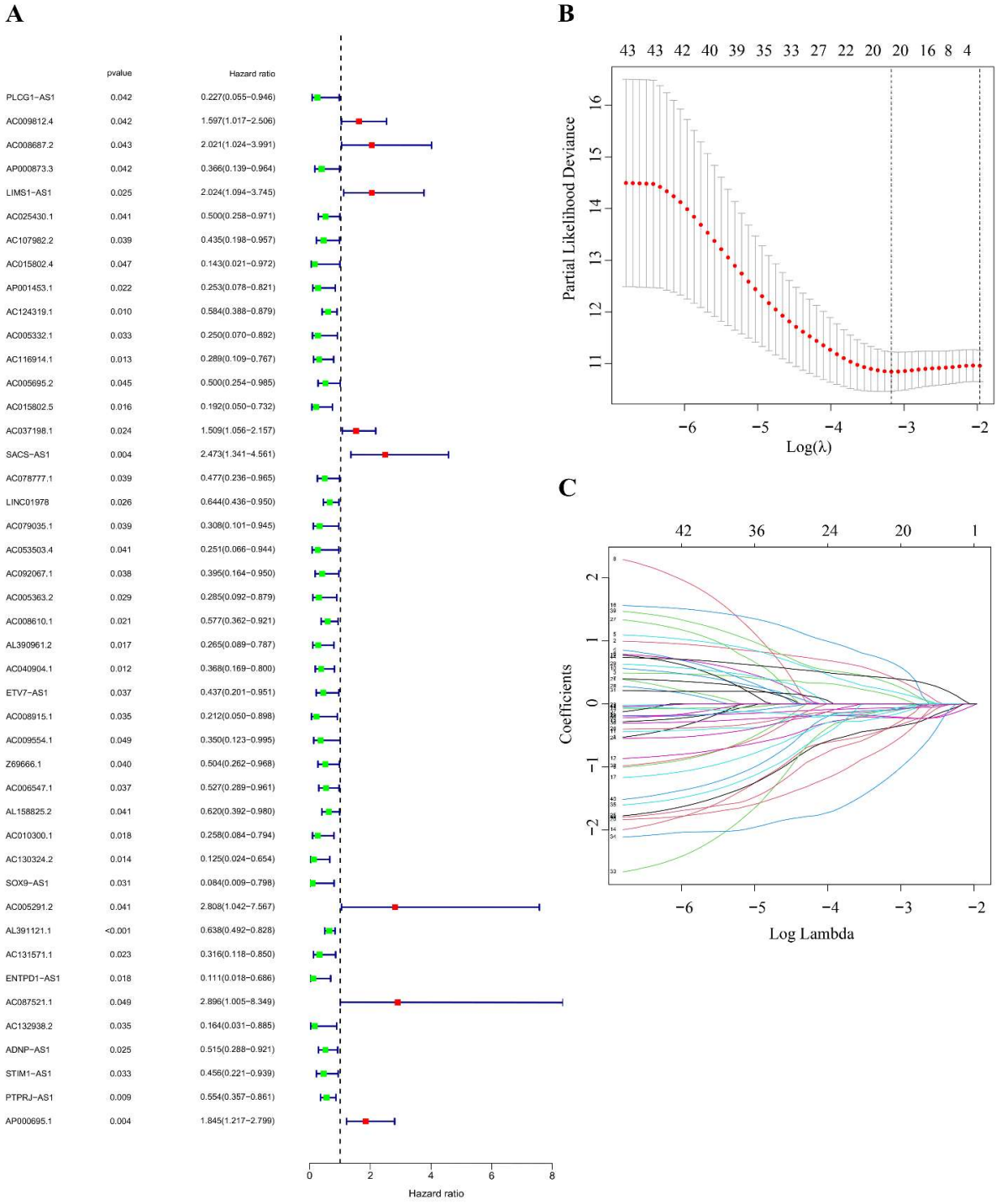

Figure 3. Establishment of the predictive model for patients with gastric cancer based on pyroptosis-associated lncRNAs. (A) Univariate Cox regression revealed significant correlations between the selected lncRNAs and clinical prognosis. A hazard ratio < 1 indicated weak risk factors; however, a hazard ratio > 1 indicated strong risk factors. (B) LASSO identified 20 pyroptosis-associated lncRNAs based on the minimum criteria when the curve was at its lowest point. (C) The coefficients of pyroptosis-associated lncRNAs according to the determined tuning parameters (log λ).

Subgroups of patients from the entire TCGA cohort were created based on sex, grade, stage or tumor phase, and the overall survivals of the low-risk subgroups were also better (Figure 6A–D). In this step, we first constructed a predictive signature and explored the predictive expression of the 10 pyroptosis-associated lncRNA signatures in the training, testing and entire cohorts, and the predictive value of this model was better evaluated.

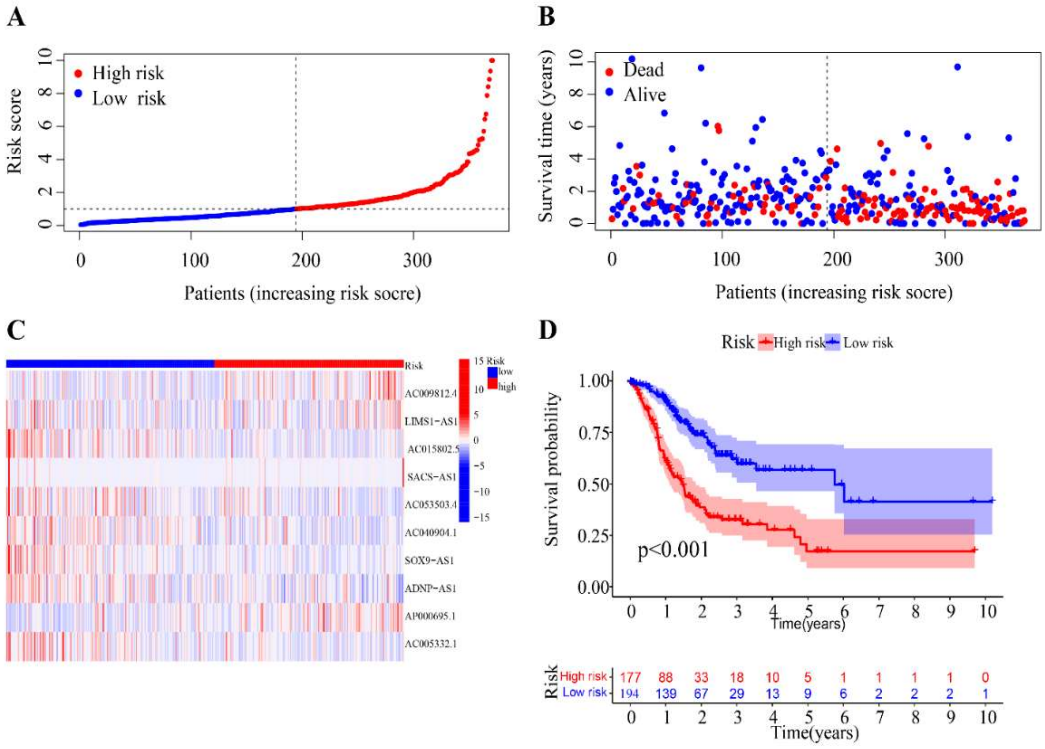

Figure 4. The predictive performances of 10 pyroptosis-associated lncRNA models in the entire cohort. (A) The distribution of the pyroptosis-associated lncRNA signature depended on the risk score for the entire cohort. Survival and death are depicted by the blue and red dots, respectively. (B) Different survival statuses and times between the two risk groups for the entire cohort. (C) The expression standards of the 10 predictive lncRNAs for every patient in the entire cohort are displayed in a heatmap created using a cluster algorithm. Red represents high expression, and blue represents low expression. (D) Kaplan–Meier analysis for the entire cohort of individuals in the two risk groups ($p < 0.001$).

3.3. Confirming the grouping efficiency of the pyroptosis-linked lncRNA signature

According to the whole gene set, 52 pyroptosis genes, 10 pyroptosis-associated lncRNAs and a predictive signature constructed by 10 pyroptosis-associated lncRNAs, principal component analysis was performed to test the differences between the two risk groups (Figure 7A–D). The locations of the two risk groups were considerably split (Figure 7A–C). In addition, the model results revealed that the two risk categories had clearly different distributions (Figure 7D). The findings showed that the predictive model could differentiate between the two risk groups, which confirmed the grouping efficiency of the signature.

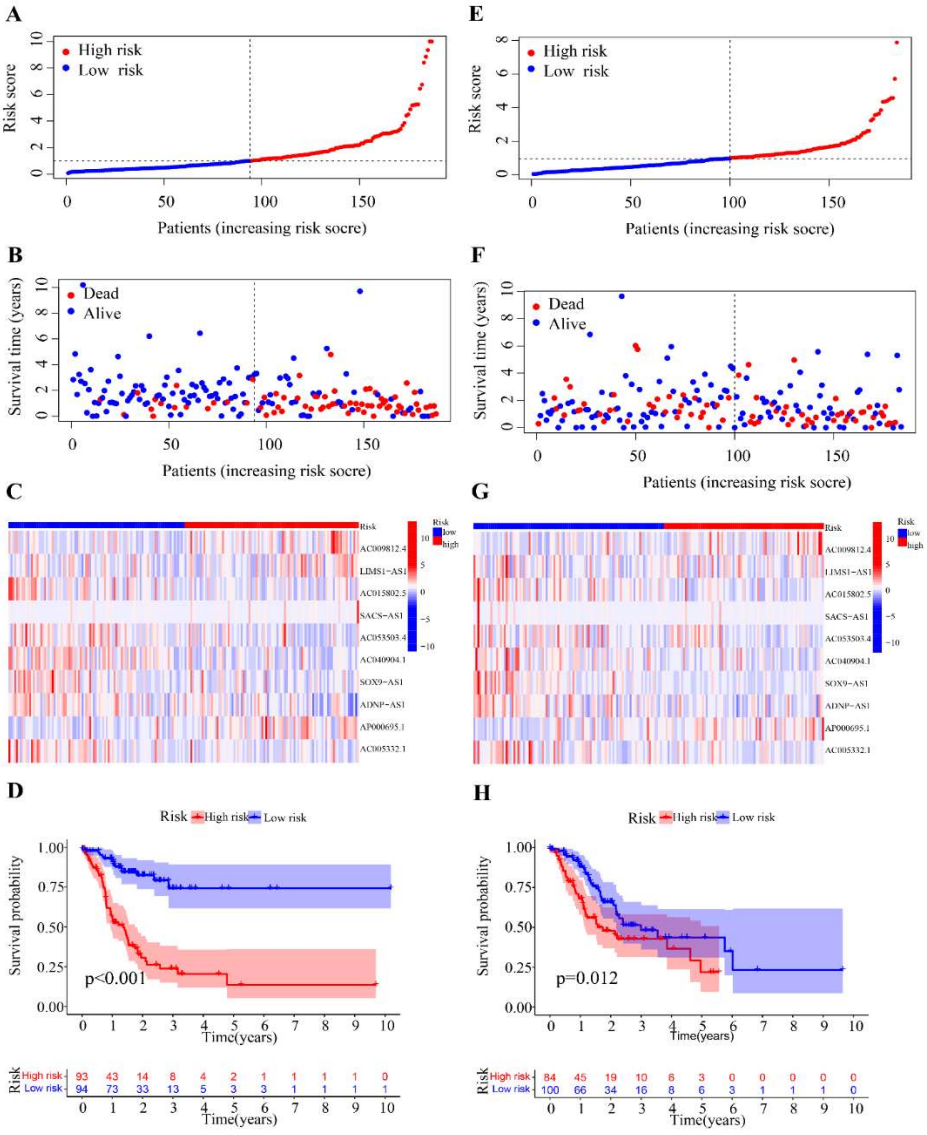

Figure 5. Predictive expression of the 10 pyroptosis-associated lncRNA signature in the training cohort and testing cohort. (A) The distribution of the pyroptosis-associated lncRNA model depended on the risk score for the training cohort. The blue and red dots represent survival and death, respectively. (B) Different survival times and statuses in the two different risk groups in the training cohort. (C) The expression levels of 10 predictive lncRNAs for every individual in the training cohort are displayed in a heatmap created by a cluster algorithm. Red represents high expression, and blue represents low expression. (D) Kaplan–Meier analysis for the training cohort of individuals in the two risk groups. (E) The distribution of the pyroptosis-associated lncRNA signature depends on the risk score for the testing cohort. Survival and death are depicted by the blue and red dots, respectively. (F) Different survival times and statuses in two different groups for the testing cohort. (G) The expression levels of 10 predictive lncRNAs for every individual in the testing cohort are displayed in a heatmap created using a cluster algorithm. Red represents high expression, and blue represents low expression. (H) Kaplan–Meier analysis of individuals in the two risk groups from the testing cohort.

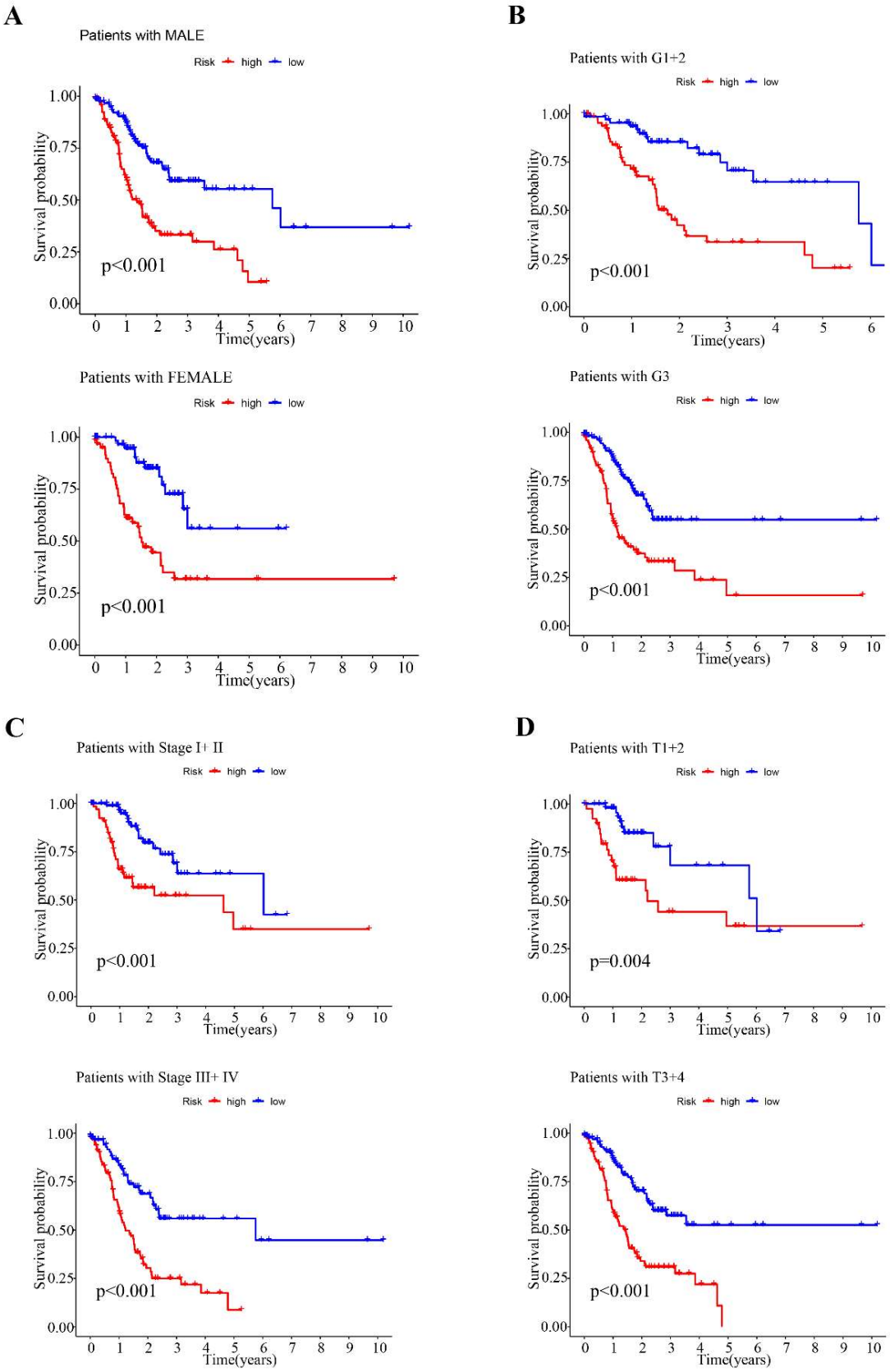

Figure 6. Kaplan–Meier curves of survival outcomes for the two risk groups in the entire TCGA cohort based on sex, grade, TNM stage (A–D) ($p < 0.01$).

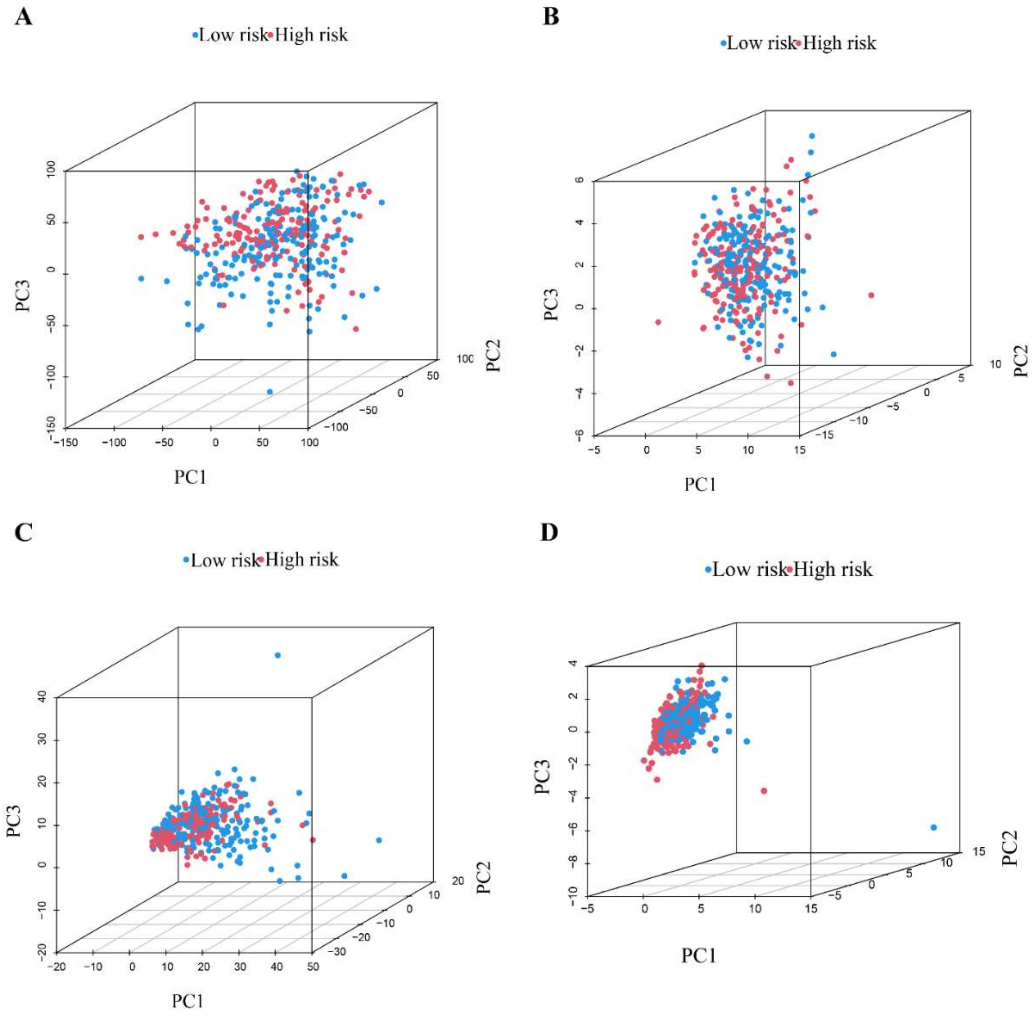

Figure 7. Principal component analysis for the two risk groups. (A) All genes. (B) Twenty-two pyroptosis-associated genes. (C) Ten pyroptosis-associated lncRNAs. (D) Risk model based on 10 pyroptosis-associated lncRNAs using the entire TCGA cohort. Red represents high risk, and blue represents low risk.

3.4. Evaluating the predictive ability of the risk model based on pyroptosis-associated lncRNAs and the clinical characteristics of GC

To determine whether the risk model based on pyroptosis-associated lncRNAs had independent predictive ability for GC, we used univariate and multivariate Cox regression. Using univariate Cox regression, the HR of the risk score was 1.132 with a 95% confidence interval (CI) of 1.090–1.175 ($p < 0.001$) (Figure 8A). The HR for pyroptosis-associated lncRNAs was 1.150 with a 95% confidence interval of 1.105–1.196 ($p < 0.001$) (Figure 8B). These results suggested that clinical and pathological factors, including sex, age, TNM stage and grade, were not connected to the risk model. The concordance index of the predictive signature increased over time, outperforming other clinical features, such as sex, age, TNM stage and grade, implying that the predictive signature could accurately predict the survival outcomes of GC patients (Figure 8C). To examine the specificity and

responsiveness of the predictive signature in forecasting the results of GC patients, the AUC was calculated. The AUC of the risk grade was greater than that of other clinical variables, indicating that the predictive ability of the risk signature was quite reliable (Figure 8D). The AUC was 0.743 at one year, 0.685 at three years and 0.715 at five years, as shown in Figure 8E. All of the above indicators demonstrated that the risk score of this predictive model was superior to other clinical characteristics.

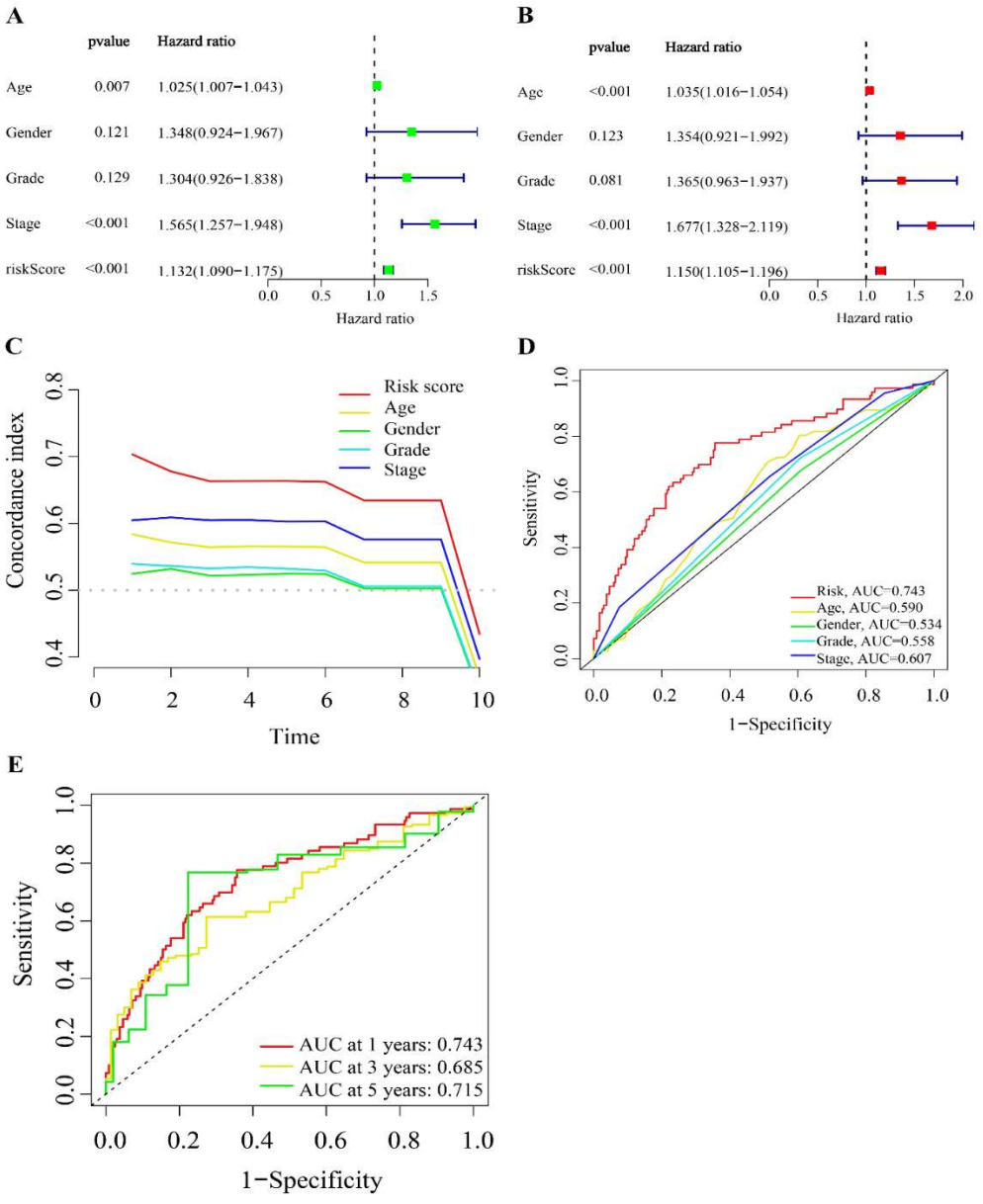

Figure 8. Evaluation of the predictive signature and clinical features in gastric cancer using the entire TCGA cohort. (A) Univariate Cox regression analysis between clinical features and risk score with survival outcome. A hazard ratio < 1 indicated weak risk factors; however, a hazard ratio > 1 indicated strong risk factors. (B) Multivariate analysis for clinical features and risk score with OS. (C) Concordance index of the risk score and clinical features. (D) ROC curves of clinical features and risk scores. (E) Time-related ROC curves of the risk model at 1, 3 and 5 years. AUC: area under the ROC curve.

3.5. Building and assessment of a predictive nomogram

This nomogram incorporating the risk score and clinical characteristics was constructed to forecast the one-, three- and five-year OS occurrences in patients with GC. Compared with clinical criteria, the risk score of the predictive signature suggested that the nomogram had better forecast power (Figure 9A). The predicting rates of the one-, three- and five-year OS exhibited perfect conformance on the correlation plot (Figure 9B). The above results indicated that the nomogram exhibited good forecasting ability.

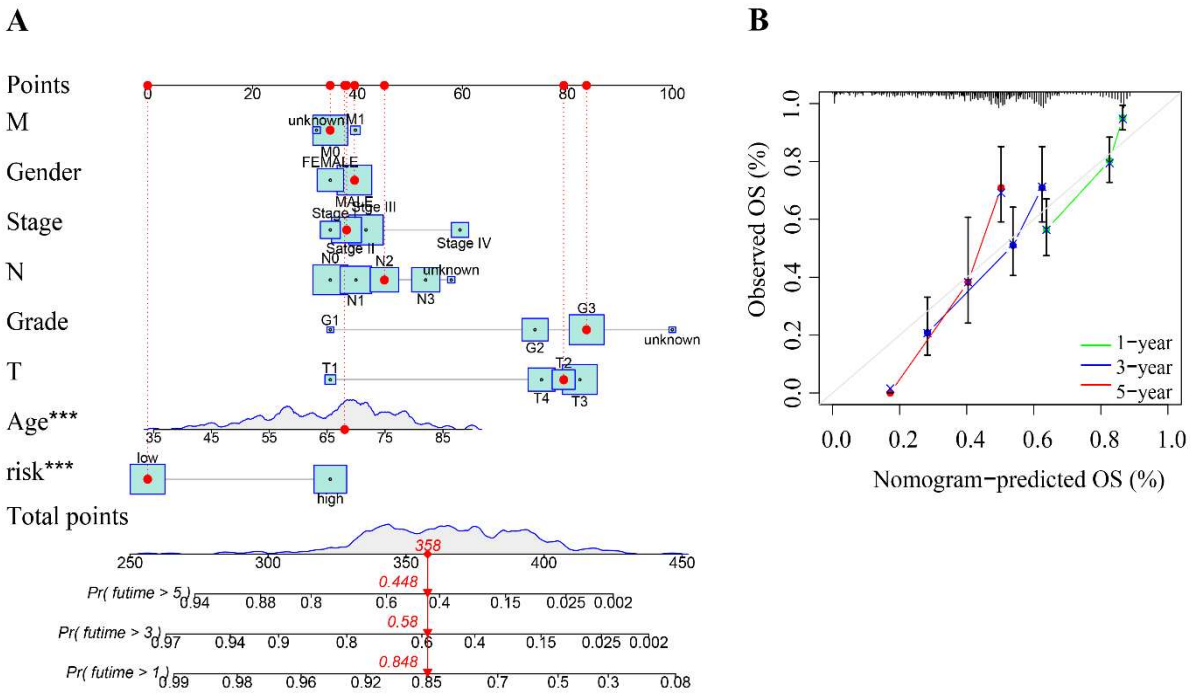

Figure 9. Building and evaluating the nomogram. (A) The nomogram predicted 1-, 3- and 5-year OS. Total points equaled the sum of the scores of each indicator, and the probability of OS was calculated based on the scores. (B) The calibration curves of the nomogram foresaw the OS at 1, 3 and 5 years. The closer the point is to the gray slash, the better the OS.

3.6. Assessment of the immune correlation and tumor immunotherapy efficacy utilizing the pyroptosis-associated lncRNA signature

Depending on the predictive signature, the enrichment degree and engagement of various immune infiltrating cells and pathways in GC were sufficiently investigated. The scores of tumor-infiltrating immune cell types in the two risk groups were determined (Figure 10A). High scores of tumors infiltrating immune cells, including DCs, iDCs, macrophages, mast cells, neutrophils, pDCs, T helper cells, TILs and Tregs, were noted in the high-risk group. We also performed ssGSEA of immune functions by comparing the two risk groups (Figure 10B). The above results showed that the high-risk group had a higher score of infiltration functions compared with the low-risk group. We performed Gene Ontology enrichment to determine the potential molecular function of the pyroptosis-associated

risk model, revealing the participation of several immune-associated biological activities (Figure S2). We found that the pyroptosis-associated genes in the risk model were mainly enriched in positive regulation of enzyme inhibitor action, peptidase mediator activity, peptidase inhibitor action, collagen-containing extracellular matrix, negative mediation of hydrolase action, regulation of peptidase action, adverse mediation of proteolysis and adverse mediation of peptidase action.

The relationship between the pyroptosis-associated lncRNA model and immunotherapeutic indicators was also explored. Gene mutations were analyzed to gain novel insight into the molecular mechanism in subgroups of the pyroptosis-associated lncRNA model. The mutation data of the pyroptosis-associated genes were evaluated using the R package maftools. Different predictors were used to classify the mutations. The top 20 driver genes (TTN, TP53, MUC16, ARID1A, LRP1B, SYNE1, FLG, FAT4, CSMD3, PCLO, DNAH5, KMT2D, FAT3, HMCN1, OBSCN, ZFHX4, RYR2, SPTA1, PIK3CA and CSMD1) with the highest mutation incidences between the two different risk subgroups are shown in Figure 10C,D. The low-risk group exhibited a greater incidence of gene mutation compared with the high-risk group (88.36 vs. 87.86%). Genes with a mutation rate of greater than 20% in the high-risk group included TTN, TP53, MUC16, ARID1A and SYNE1. TTN, TP53, MUC16, ARID1A, LRP1B, SYNE1, FLG, FAT4, CSMD3 and PCLO were identified as genes with mutation rates of greater than 20% in the low-risk subgroups. The most common mutation in both groups was Missense_mutation followed by Multi_Hit, Frame_Shift_Del and Nonsense_ mutation.

In many malignancies, including gastric cancer, a connection is noted between treatment intervention and TMB. The higher the TMB score is, the more cancer genetic mutations. In addition, a higher TMB score was noted in tumors with more abnormal cells. Thus, it was possible for immune cells to find the tumor. This type of tumor was a good candidate for tumor immunological treatment. We then calculated tumor mutational burden scores using the mutation data. The TMB in the high-risk category was lower, demonstrating that pyroptosis-associated factors exhibited a stronger relationship with the TMB (Figure 10E). Gastric cancer patients with a high TMB score had a considerably greater survival rate (Figure 10F). The above results indicated that TMB could act as an independent predictive factor in gastric cancer. Then, we tested whether the risk model could predict the OS of GC patients together with tumor mutational burden. Patients with two different TMB scores in the high-risk category (called H-TMB/high and L-TMB/high) had a lower survival rate than individuals with the two different TMB groups in the low-risk category (H-TMB/low and L-TMB/low) (Figure 10G). Based on our findings, the pyroptosis-associated lncRNA model could have increased predictive value with tumor mutational burden. The above results implied that immune infiltrating levels, mutation incidence and TMB significantly differed in the two risk groups, and this information can be used to guide individual treatment.

3.7. Drug sensitivity assessment based on pyroptosis-associated lncRNAs in patients with gastric cancer

We used a drug sensitivity analysis to assess the IC_{50} differences between risk categories from the GDSC database to identify a better chemotherapy regimen for GC patients. With the exception of ABT.888 and AKT inhibitor VIII, the low-risk group was more responsive to A.443654, A.770041, AICAR, AMG.706, AS601245, ATRA, AUY922, axitinib, AZ628 and AZD.0530 (Figure 11A–L). We hypothesized that the effect of adequate treatment was superior in high-risk populations and that the information derived from these studies would be useful to guide individual chemotherapy.

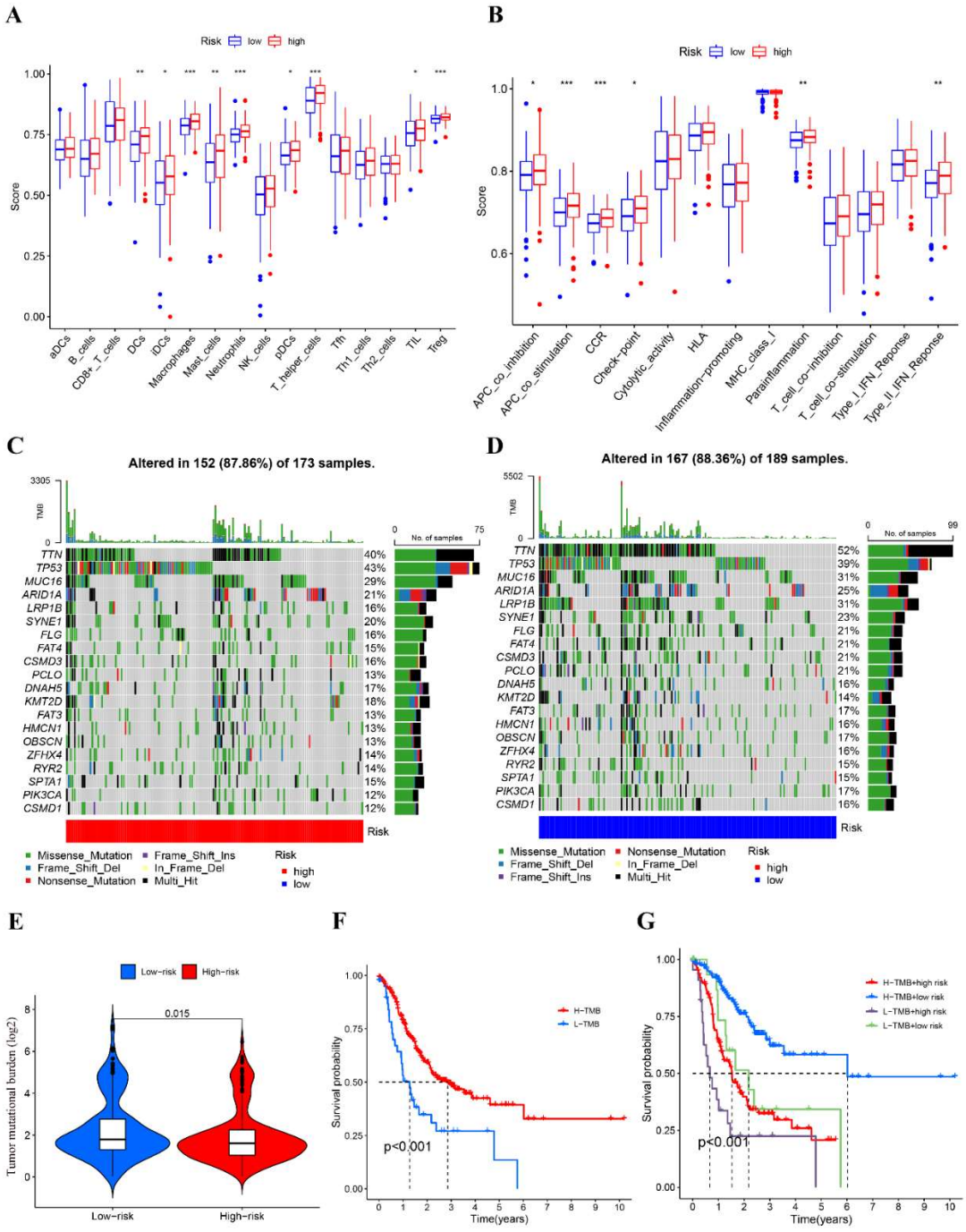

Figure 10. Assessment of tumor immune correlation and tumor immunotherapy efficacy using the pyroptosis-associated lncRNA signature. (A) The scores of tumor-infiltrating immune cell types in the two risk groups. (B) The scores of immune functions were compared in the two risk groups using ssGSEA. Different mutation rates in the high-risk group (C) and low-risk group (D) are presented in waterfall curves. BP: biological process; CC: cellular component; MF: molecular function. (E) TMB differences in the individuals of the two risk groups. (F) Kaplan–Meier analysis of patients with different TMB levels. (G) Kaplan–Meier analysis of survival outcomes for individuals based on TMB levels and the pyroptosis-associated lncRNA model is shown.

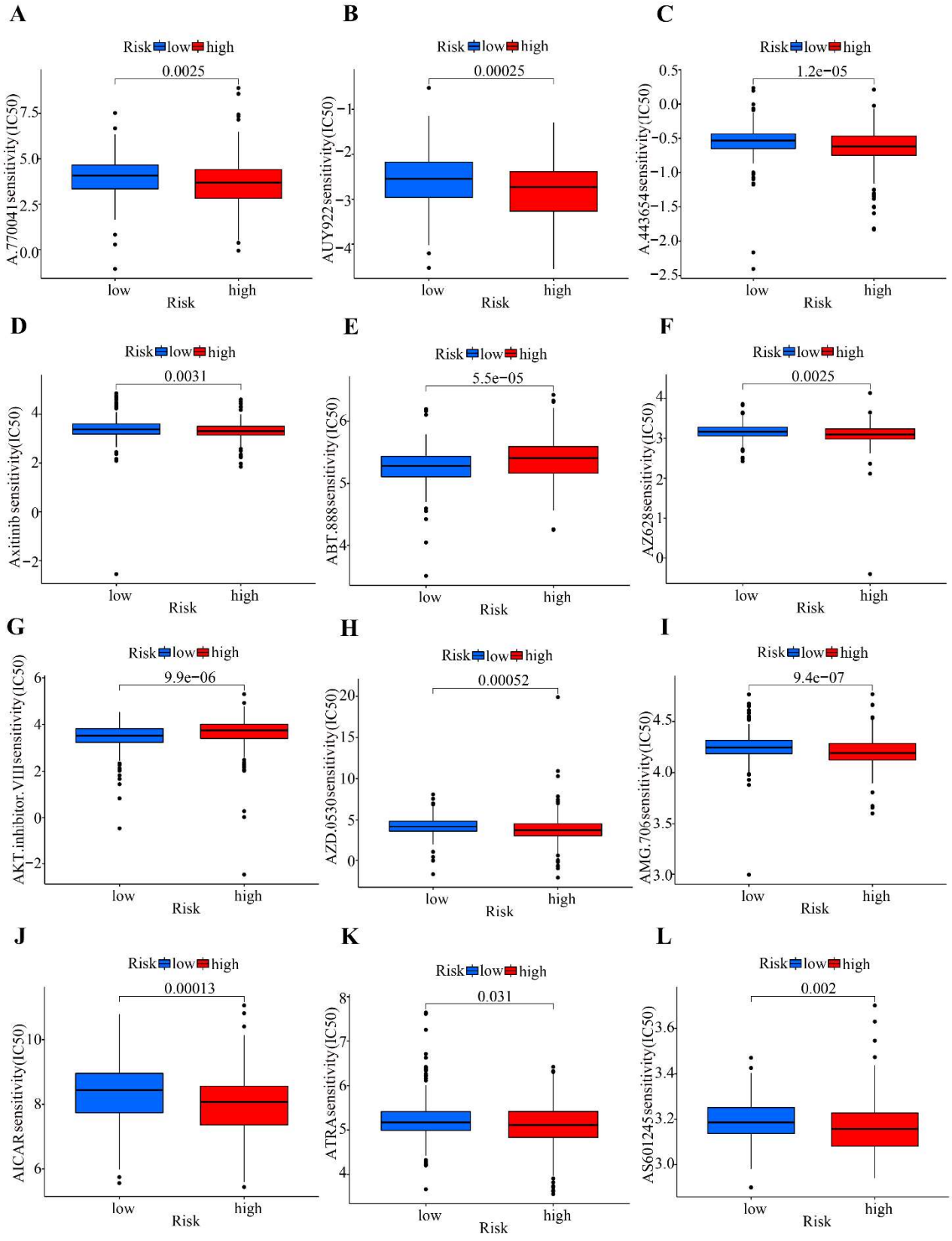

Figure 11. Assessment of drug sensitivity (IC_{50}) in patients with GC. IC_{50}: the half maximal inhibitory concentration (A–L).

3.8. Expression levels of hub pyroptosis-associated lncRNAs in patients with GC

We further explored the expression of hub pyroptosis-associated lncRNAs in the lnCAR database. The results indicated that AC005332.1, AC009812.4 and AP000695.1 levels were significantly increased in gastric tumor tissue compared with normal tissue (Figure 12A–C). And the overall survival of the patients with GC had statistically significant in high and low AP000695.1 group ($p < 0.05$) (Figure 12D). These results were consistent with the results based on TCGA GC cohort, demonstrating that AC005332.1, AC009812.4 and AP000695.1 were crucial biomarkers in regulating GC progression. The above results provide novel ideas to explore the specific mechanisms of the initiation and development of gastric cancer.

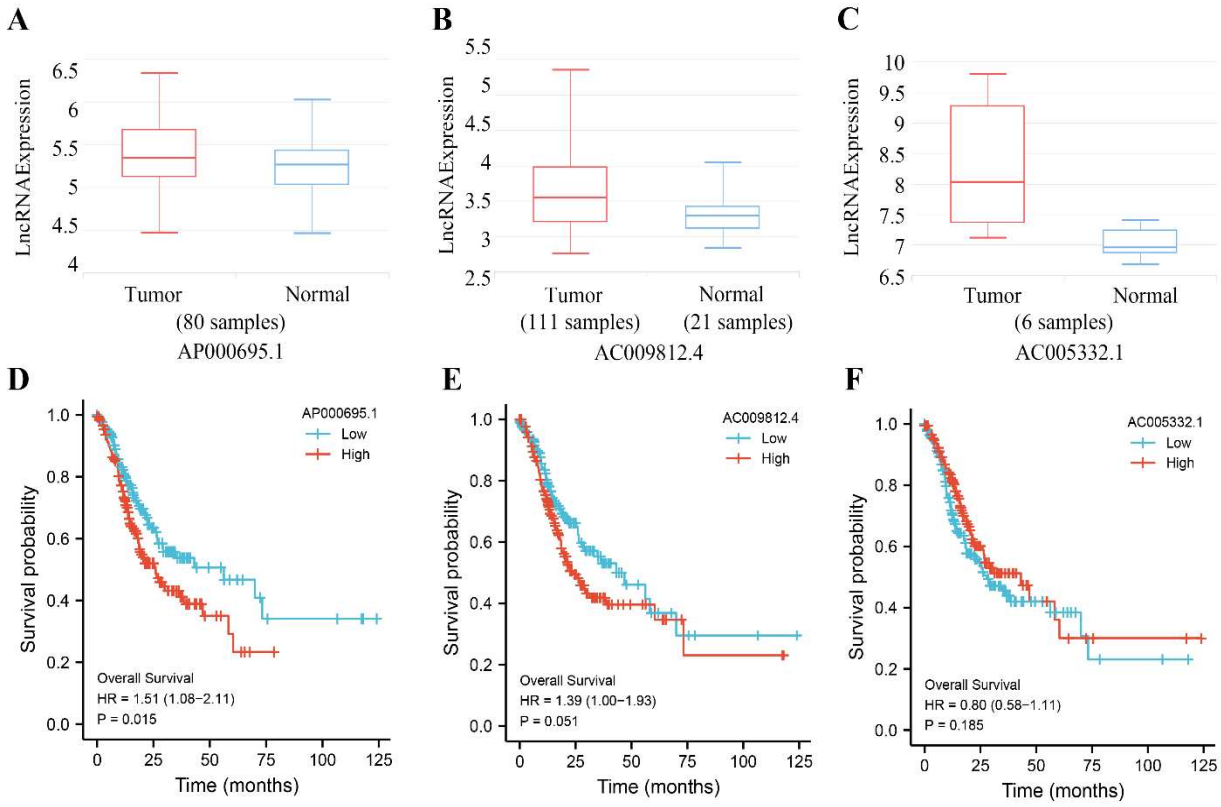

Figure 12. The expression levels and overall survival of hub pyroptosis-associated lncRNAs in the patients with GC. (A–C) The expression levels of AC009812.4, AP000695.1 and AC005332.1 in the lnCAR database. (D–F) The overall survival of AC009812.4, AP000695.1 and AC005332.1 in the Sento Academic website. *$p < 0.05$. **$p < 0.01$. ***$p < 0.001$.

4. Discussion

GC is well known as a common gastrointestinal system tumor with a high morbidity and mortality rate, and it receives an increasing amount of attention each year [48]. A reliable method to correctly predict the outcomes of GC patients is currently not available. In addition, pyroptosis has a dual effect

on the appearance and growth of cancers. Pyroptotic cell death in the oxygen-deficit area of the tumor center could impair antitumor immunity and facilitate tumor formation [26]. On the other hand, pyroptosis can trigger an immune reaction and slow tumor development by causing acute inflammation in the tumor microenvironment [49]. For example, the AIM2 inflammasome has been shown to regulate mTOR to diminish S6K1 activation, thereby suppressing tumor progression [50]. However, the interaction of pyroptosis-associated genes in GC and their underlying potential to forecast GC patient prognosis remain unknown.

Furthermore, the critical role of lncRNAs in the induction of pyroptosis in tumor cells has been verified. For instance, previous work focused on GSDME to investigate the crucial function of lncRNAs involved in ionizing radiation (IR)-regulated pyroptosis in colon cancer cells [51]. The findings shed light on the biochemical processes driving IR-induced damage in cancer radiation treatment and could provide a solid theoretical framework for the development of colon cancer treatments. Furthermore, microRNA-4306 and Sirtuin1 (SIRT1) regulate the expression of LINC00958, which is involved in the induction of oral squamous cell carcinoma cell death by missing in melanoma 2 [52]. Nevertheless, research on lncRNAs connected to pyroptosis in tumors, particularly GC, is severely poor. As a result, we aimed to develop a predictive model based on pyroptosis-associated lncRNAs in patients with gastric cancer with the goal of generating a model that could accurately predict the outcomes of GC patients and provide a promising treatment option in the future.

The purpose of our study was to identify the association between pyroptosis-associated lncRNAs and GC patient outcome based on the expression data and biological activity of pyroptosis-associated lncRNAs in GC. Pyroptosis-associated lncRNAs were identified through co-expression analyses. To create a pyroptosis-associated lncRNA risk model, we used LASSO for univariate and multivariate Cox regression. The predictive signature comprising 10 pyroptosis-associated lncRNAs (AC005332.1, AC009812.4, AC015802.5, AC040904.1, AC053503.4, ADNP−AS1, AP000695.1, LIMS1−AS1, SACS−AS1 and SOX9−AS1) was confirmed to be an independent factor of prognosis. Among the 10 lncRNAs of the predictive model, several pyroptosis-associated lncRNAs have been reported to facilitate tumor incidence and progression. For example, a SOX9-AS1/miR-5590-3p/SOX9 positive feedback loop that signals through the Wnt/β-catenin pathway causes the progression and metastasis of HCC, suggesting that SOX9-AS1 represents a promising new predictive and therapeutic target for HCC [53]. Therefore, more researchers would like to study the role of pyroptosis-associated lncRNAs in GC and assess their value as predictive indicators.

Our study also discovered that this risk model was closely connected with immunotherapeutic markers and the prediction of sensitivity to medication. Various immunological biomarkers differed between the two risk groups. The above outcomes further showed that the pyroptosis-associated lncRNA model had a significant effect on the immune cell-infiltrating environment. We can focus more on the high-risk group because in the high-risk group, immune cells as well as immune function have higher scores. Relationships between treatment efficacy and TMB are noted in many malignancies, including gastric cancer. The TMB was higher in the low-risk group, demonstrating that the pyroptosis-associated signature was closely related to TMB. The survival probability of GC patients in the high TMB group was increased. TMB was identified as a risk-independent predictive marker in gastric cancer based on the findings of this study. The IC_{50} in the GDSC database was compared between risk categories using a drug susceptibility assessment. We found that the effect of adequate treatment is superior in high-risk populations. Finally, we further explored the expression of hub pyroptosis-

associated lncRNAs in the lnCAR database.

The pathogenic stage is an important factor in the decision regarding GC treatment. However, GC patients in the same pathological stage also exhibit diverse clinical results, demonstrating that earlier categorization approaches are ineffective in providing reliable predictions and distinguishing the heterogeneity of GC. As a result, the established pyroptosis-associated lncRNA model provides a novel and accurate method to predict the survival outcomes and immunological responses of GC patients. We also validated the above results using the lnCAR database. The novelty of our work lies in the combination of two factors (pyroptosis and lncRNA) that play an important role in gastric cancer to establish a new prediction model. The main contribution is that, currently, earlier staging methods are ineffective in providing reliable predictions and facilitating the differentiation of gastric cancer heterogeneity based on a multitude of bioinformatics and computer algorithms. Here, we constructed and validated a prediction model to provide an accurate and simple method to predict patient survival and provide a theoretical basis for patient treatment. The model can be reproduced, making it attractive for clinical translation and implementation. Despite the significant findings of our study, we note that our research had several flaws and limitations. Research on the correlation between pyroptosis-linked lncRNAs and the tumor immune microenvironment remains in its initial phases and requires a more thorough analysis. Moreover, an *in vivo* test was used to confirm the expression activity of pyroptosis-associated lncRNAs. Based on the above results, we constructed a prognostic model consisting of 10 pyroptosis-linked lncRNAs. Recently, ncRNAs, including lncRNAs, miRNAs and circRNAs, have attracted considerable attention from scientists [54]. Prediction studies focused on interacting factors will provide valuable insights into the genetic markers and ncRNAs associated with GC, such as the lncRNA-miRNA-mRNA ceRNA network [55–57] and circRNA-miRNA-mRNA network [58]. Ideally, the simultaneous use of several correlated molecular targets increases the sensitivity and reliability of candidate genes as biomarkers [59], which also represents the direction of our future research.

5. Conclusions

In conclusion, we developed an excellent risk model to forecast the outcomes of GC patients based on 10 pyroptosis-associated lncRNAs, including AC005332.1, AC009812.4, AC015802.5, AC040904.1, AC053503.4, ADNPAS1, AP000695.1, LIMS1AS1, SACSAS1 and SOX9AS1. Validation results showed that AC005332.1, AC009812.4 and AP000695.1 were crucial biomarkers in regulating GC progression. And the overall survival of the patients with GC had statistically significant in high and low AP000695.1 group. More importantly, the above findings could elucidate the function of pyroptosis-associated lncRNAs and provide adequate evidence for prognostic prediction in GC patients. Furthermore, the predictive risk model demonstrated efficacy in identifying GC patients who would benefit from immunotherapy.

Acknowledgments

Jinsong Liu and Wenbin Lu designed this work. Yuyang Dai and Qian Liu integrated and analyzed the data. Jinsong Liu wrote this manuscript. Yueyao Lu, Jianzhong Deng and Xiuling Liu edited and modified the manuscript. This manuscript was approved by all of the authors.

This research project was funded by the National Natural Science Foundation of China [grant number 81872275], Medical Research Project of Jiangsu Health Commission [M2020002], the

Changzhou High-Level Medical Talents Training Project [No: 2016CZBJ054] and the funds of Changzhou Sci & Tech Program [grant numbers CJ20220007, CJ20220006, CJ20210015].

Ethics statement

The data from the public database are open access, and this study does not need the approval of the clinical ethics committee. The study complied with the corresponding rules of the public database.

Conflict of interest

The authors have no conflicts of interest to disclose.

References

1. Y. Shao, H. Jia, S. Li, L. Huang, B. Aikemu, G. Yang, et al., Comprehensive analysis of ferroptosis-related markers for the clinical and biological value in gastric cancer, *Oxid. Med. Cell. Longev*., **2021** (2021), 7007933. https://doi.org/10.1155/2021/7007933
2. H. Sung, J. Ferlay, R. L. Siegel, M. Laversanne, I. Soerjomataram, A. Jemal, et al., Global Cancer Statistics 2020: GLOBOCAN estimates of incidence and mortality worldwide for 36 cancers in 185 countries, *CA Cancer J. Clin*., **71** (2021), 209–249. https://doi.org/10.3322/caac.21660
3. E. C. Smyth, M. Nilsson, H. IGrabsch, N. C. T. van Grieken, F. Lordick, Gastric cancer, *Lancet*, **396** (2020), 635–648. https://doi.org/10.1016/S0140-6736(20)31288-5
4. F. Lordick, K. Shitara, Y. Y. Janjigian, New agents on the horizon in gastric cancer, *Ann. Oncol.*, **28** (2017), 1767–1775. https://doi.org/10.1093/annonc/mdx051
5. Y. Liu, N. S. Sethi, T. Hinoue, B. G. Schneider, A. D. Cherniack, F. Sanchez-Vega, et al., Comparative molecular analysis of gastrointestinal adenocarcinomas, *Cancer Cell*, **33** (2018), 721–735. https://doi.org/10.1016/j.ccell.2018.03.010
6. The Cancer Genome Atlas Research Network, Comprehensive molecular characterization of gastric adenocarcinoma, *Nature*, **513** (2014), 202–209. https://doi.org/10.1038%2Fnature13480
7. Y. Tan, Q. Chen, X. Li, Z. Zeng, W. Xiong, G. Li, et al., Pyroptosis: a new paradigm of cell death for fighting against cancer, *J. Exp. Clin. Cancer Res.*, **40** (2021), 153. https://doi.org/10.1186/s13046-021-01959-x
8. X. Liu, S. Xia, Z. Zhang, H. Wu, J. Lieberman, Channelling inflammation: gasdermins in physiology and disease, *Nat. Rev. Drug Discov.*, **20** (2021), 384–405. https://doi.org/10.1038/s41573-021-00154-z
9. J. Shi, W. Gao, F. Shao, Pyroptosis: Gasdermin-mediated programmed necrotic cell death, *Trends Biochem. Sci.*, **42** (2017), 245–254. https://doi.org/10.1016/j.tibs.2016.10.004
10. Z. Zeng, G. Li, S. Wu, Z. Wang, Role of pyroptosis in cardiovascular disease, *Cell Prolif.*, **52** (2019), e12563. https://doi.org/10.1111/cpr.12563
11. J. Yu, S. Li, J. Qi, Z. Chen, Y. Wu, J. Guo, et al., Cleavage of GSDME by caspase-3 determines lobaplatin-induced pyroptosis in colon cancer cells, *Cell Death Dis.*, **10** (2019), 193. https://doi.org/10.1038/s41419-019-1441-4

12. C. Lin, L. Yang, Long noncoding RNA in cancer: Wiring signaling circuitry, *Trends Cell Biol.*, **28** (2018), 287–301. https://doi.org/10.1016/j.tcb.2017.11.008
13. J. J. Quinn, H. Y. Chang, Unique features of long non-coding RNA biogenesis and function, *Nat. Rev. Genet.*, **17** (2016), 47–62. https://doi.org/10.1038/nrg.2015.10
14. Y. Huang, J. Zhang, L. Hou, G. Wang, H. Liu, R. Zhang, et al., LncRNA AK023391 promotes tumorigenesis and invasion of gastric cancer through activation of the PI3K/Akt signaling pathway, *J. Exp. Clin. Cancer Res.*, **36** (2017), 194. https://doi.org/10.1186/s13046-017-0666-2
15. G. Zhang, S. Li, J. Lu, Y. Ge, Q. Wang, G. Ma, et al., LncRNA MT1JP functions as a ceRNA in regulating FBXW7 through competitively binding to miR-92a-3p in gastric cancer, *Mol. Cancer*, **17** (2018), 87. https://doi.org/10.1186/s12943-018-0829-6
16. H. T. Liu, S. Liu, L. Liu, R. R. Ma, P. Gao, EGR1-mediated transcription of lncRNA-HNF1A-AS1 promotes cell-cycle progression in gastric cancer, *Cancer Res.*, **78** (2018), 5877–5890. https://doi.org/10.1158/0008-5472.CAN-18-1011
17. M. Arunkumar, C. E. Zielinski, T-Cell receptor repertoire analysis with computational tools-an immunologist's perspective, *Cells*, **10** (2021), 3582.
18. F. Sun, J. Sun, Q. Zhao, A deep learning method for predicting metabolite-disease associations via graph neural network, *Briefings Bioinf.*, **23** (2022), bbac266. https://doi.org/10.1093/bib/bbac266
19. R. C. Deo, Machine learning in medicine, *Circulation*, **132** (2015), 1920–1930. https://doi.org/10.1161/CIRCULATIONAHA.115.001593
20. C. Bock, T. Lengauer, Computational epigenetics, *Bioinformatics*, **24** (2008), 1–10. https://doi.org/10.1093/bioinformatics/btm546
21. F. Xu, X. Huang, Y. Li, Y. Chen, L. Lin, m(6)A-related lncRNAs are potential biomarkers for predicting prognoses and immune responses in patients with LUAD, *Mol. Ther. Nucleic Acids*, **24** (2021), 780–791. https://doi.org/10.1016/j.omtn.2021.04.003
22. D Zheng, L Yu, Z Wei, K Xia, W Guo, N6-methyladenosine-related lncRNAs are potential prognostic biomarkers and correlated with tumor immune microenvironment in osteosarcoma, *Front. Genet.*, **12** (2021), 805607.
23. X. Guo, W. Zhong, Y. Chen, W. Zhang, J. Ren, A. Gao, Benzene metabolites trigger pyroptosis and contribute to haematotoxicity via TET2 directly regulating the Aim2/Casp1 pathway, *EBioMedicine*, **47** (2019), 578–589. https://doi.org/10.1016/j.ebiom.2019.08.056
24. F. F. S. Ke, H. K. Vanyai, A. D. Cowan, A. R. D. Delbridge, L. Whitehead, S. Grabow, et al., Embryogenesis and adult life in the absence of intrinsic apoptosis effectors BAX, BAK, and BOK, *Cell*, **173** (2018), 1217–1230.e17. https://doi.org/10.1016/j.cell.2018.04.036
25. J. Shi, Y. Zhao, K. Wang, X. Shi, Y. Wang, H. Huang, et al., Cleavage of GSDMD by inflammatory caspases determines pyroptotic cell death, *Nature*, **526** (2015), 660–665. https://doi.org/10.1038/nature15514
26. Y. Fang, S. Tian, Y. Pan, W. Li, Q. Wang, Y. Tang, et al., Pyroptosis: A new frontier in cancer, *Biomed. Pharmacother.*, **121** (2020), 109595. https://doi.org/10.1016/j.biopha.2019.109595
27. Z. Li, Y. Jia, Y. Feng, R. Cui, R. Miao, X. Zhang, et al., Methane alleviates sepsis-induced injury by inhibiting pyroptosis and apoptosis: In vivo and in vitro experiments, *Aging*, **11** (2019), 1226–1239. https://doi.org/10.18632%2Faging.101831

28. B. Liu, R. He, L. Zhang, B. Hao, W. Jiang, W. Zhang, et al., Inflammatory caspases drive pyroptosis in acute lung injury, *Front. Pharmacol.*, **12** (2021), 631256. https://doi.org/10.3389/fphar.2021.631256
29. D. D. Tian, M. Wang, A. Liu, M. R. Gao, C. Qiu, W. Yu, et al., Antidepressant effect of paeoniflorin is through inhibiting pyroptosis CASP-11/GSDMD pathway, *Mol. Neurobiol.*, **58** (2021), 761–776. https://doi.org/10.1007/s12035-020-02144-5
30. Y. L. Gao, J. H. Zhai, Y. F. Chai, Recent advances in the molecular mechanisms underlying pyroptosis in sepsis, *Mediators Inflamm*, **2018** (2018), 5823823. https://doi.org/10.1155/2018/5823823
31. K. S. Schneider, C. J. Groß, R. F. Dreier, B. S. Saller, R. Mishra, O. Gorka, et al., The inflammasome drives GSDMD-independent secondary pyroptosis and IL-1 release in the absence of Caspase-1 protease activity, *Cell Rep.*, **21** (2017), 3846–3859. https://doi.org/10.1016/j.celrep.2017.12.018
32. A. Malik, T. D. Kanneganti, Inflammasome activation and assembly at a glance, *J. Cell Sci.*, **130** (2017), 3955–3963. https://doi.org/10.1242/jcs.207365
33. E. Scosyrev, E. Glimm, Power analysis for multivariable Cox regression models, *Stat. Med.*, **38** (2019), 88–99. https://doi.org/10.1002/sim.7964
34. P. C. Schober, C. Boer, L. A. Schwarte, Correlation coefficients: Appropriate use and interpretation, *Anesth. Analg.*, **126** (2018), 1763–1768. https://doi.org/10.1213/ANE.0000000000002864
35. S. Xu, D. Liu, T. Chang, X. Wen, S. Ma, G. Sun, et al., Cuproptosis-associated lncRNA establishes new prognostic profile and predicts immunotherapy response in clear cell renal cell carcinoma, *Front. Genet.*, **13** (2022), 938259. https://doi.org/10.3389%2Ffgene.2022.938259
36. X. Ma, C. Mo, L. Huang, P. Cao, L. Shen, C. Gui, An robust rank aggregation and least absolute shrinkage and selection operator analysis of novel gene signatures in dilated cardiomyopathy, *Front. Cardiovasc. Med.*, **8** (2021), 747803. https://doi.org/10.3389%2Ffcvm.2021.747803
37. X. Liu, D. Wang, S. Han, F. Wang, Z. Zang, C. Xu, et al., Signature of m5C-Related lncRNA for prognostic prediction and immune responses in pancreatic cancer, *J. Oncol.*, **2022** (2022), 7467797. https://doi.org/10.1155/2022/7467797
38. Y. Li, J. Wang, F. Wang, C. Gao, Y. Cao, J. Wang, et al., Development and verification of an autophagy-related lncRNA signature to predict clinical outcomes and therapeutic responses in ovarian cancer, *Front. Med.*, **8** (2021), 715250. https://doi.org/10.3389/fmed.2021.715250
39. J. X. Mi, Y. N. Zhang, Z. Lai, W. Li, L. Zhou, F. Zhong, Principal component analysis based on nuclear norm minimization, *Neural Networks*, **118** (2019), 1–16. https://doi.org/10.1016/j.neunet.2019.05.020
40. S. Lacny, T. Wilson, F. Clement, D. J. Roberts, P. Faris, W. A. Ghali, et al., Kaplan-Meier survival analysis overestimates cumulative incidence of health-related events in competing risk settings: a meta-analysis, *J. Clin. Epidemiol.*, **93** (2018), 25–35. https://doi.org/10.1016/j.jclinepi.2017.10.006
41. J. Y. Ma, S. Liu, J. Chen, Q. Liu, Metabolism-related long non-coding RNAs (lncRNAs) as potential biomarkers for predicting risk of recurrence in breast cancer patients, *Bioengineered*, **12** (2021), 3726–3736. https://doi.org/10.1080/21655979.2021.1953216
42. Y. Wang, J. Li, Y. Xia, R. Gong, K. Wang, Z. Yan, et al., Prognostic nomogram for intrahepatic cholangiocarcinoma after partial hepatectomy, *J. Clin. Oncol.*, **31** (2013), 1188–1195.

43. W. Lv, Y. Tan, C. Zhao, Y. Wang, M. Wu, Y. Wu, et al., Identification of pyroptosis-related lncRNAs for constructing a prognostic model and their correlation with immune infiltration in breast cancer, *J. Cell. Mol. Med.*, **25** (2021), 10403–10417. https://doi.org/10.1111/jcmm.16969
44. M. Li, W. Cao, B. Huang, Z. Zhu, Y. Chen, J. Zhang, et al., Establishment and analysis of an individualized immune-related gene signature for the prognosis of gastric cancer, *Front. Surg.*, **9** (2022), 829237. https://doi.org/10.3389/fsurg.2022.829237
45. Y. Chen, C. Zhang, X. Zou, M. Yu, B. Yang, C. F. Ji, et al., Identification of macrophage related gene in colorectal cancer patients and their functional roles, *BMC Med. Genomics*, **14** (2021), 159. https://doi.org/10.1186/s12920-021-01010-0
46. W. Yang, J. Soares, P. Greninger, E. J. Edelman, H. Lightfoot, S. Forbes, et al., Genomics of drug sensitivity in cancer (GDSC): A resource for therapeutic biomarker discovery in cancer cells, *Nucleic Acids Res.*, **41** (2013), 955–961. https://doi.org/10.1093/nar/gks1111
47. Y. Zheng, Q. Xu, M. Liu, H. Hu, Y. Xie, Z. Zuo, et al., lnCAR: A comprehensive resource for lncRNAs from cancer arrays, *Cancer Res.*, **79** (2019), 2076–2083. https://doi.org/10.1158/0008-5472.CAN-18-2169
48. T. Han, D. Xu, J. Zhu, J. Li, L. Liu, Y. Deng, Identification of a robust signature for clinical outcomes and immunotherapy response in gastric cancer: Based on N6-methyladenosine related long noncoding RNAs, *Cancer Cell Int.*, **21** (2021), 432. https://doi.org/10.1186/s12935-021-02146-w
49. S. Kesavardhana, R. K. S. Malireddi, T. D. Kanneganti, Caspases in cell death, inflammation, and gasdermin-induced pyroptosis, *Annu. Rev. Immunol.*, **38** (2020), 567–595. https://doi.org/10.1146%2Fannurev-immunol-073119-095439
50. X. Ma, P. Guo, Y. Qiu, K. Mu, L. Zhu, W. Zhao, et al., Loss of AIM2 expression promotes hepatocarcinoma progression through activation of mTOR-S6K1 pathway, *Oncotarget*, **7** (2016), 36185–36197. https://doi.org/10.18632%2Foncotarget.9154
51. F. Su, J. Duan, J. Zhu, H. Fu, X. Zheng, C. Ge, Long noncoding RNA nuclear paraspeckle assembly transcript 1 regulates ionizing radiationinduced pyroptosis via microRNA448/gasdermin E in colorectal cancer cells, *Int. J. Oncol.*, **59** (2021), 1–11. https://doi.org/10.3892%2Fijo.2021.5259
52. L. Jiang, W. Ge, Y. Cui, Z. Wang, The regulation of long non-coding RNA 00958 (LINC00958) for oral squamous cell carcinoma (OSCC) cells death through absent in melanoma 2 (AIM2) depending on microRNA-4306 and Sirtuin1 (SIRT1) in vitro, *Bioengineered*, **12** (2021), 5085–5098. https://doi.org/10.1080/21655979.2021.1955561
53. W. Zhang, Y. Wu, B. Hou, Y. Wang, D. Deng, Z. Fu, et al., A SOX9-AS1/miR-5590-3p/SOX9 positive feedback loop drives tumor growth and metastasis in hepatocellular carcinoma through the Wnt/beta-catenin pathway, *Mol. Oncol.*, **13** (2019), 2194–2210. https://doi.org/10.1002/1878-0261.12560
54. C. Wang, C. D. Han, Q. Zhao, X. Chen, Circular RNAs and complex diseases: from experimental results to computational models, *Brief. Bioinf.*, **22** (2021), bbab286. https://doi.org/10.1093/bib/bbab286
55. Y. Wang, X. Huang, S. Chen, H. Jiang, H. Rao, L. Lu, et al., In Silico identification and validation of cuproptosis-related lncRNA signature as a novel prognostic model and immune function analysis in colon adenocarcinoma, *Curr. Oncol.*, **29** (2022), 6573–6593. https://doi.org/10.3390/curroncol29090517

56. L. Zhang, T. Liu, H. Chen, Q. Zhao, H. Liu, Predicting lncRNA-miRNA interactions based on interactome network and graphlet interaction, *Genomics*, **113** (2021), 874–880. https://doi.org/10.1016/j.ygeno.2021.02.002
57. L. Zhang, P. Yang, H. Feng, Q. Zhao, H. Liu, Using network distance analysis to predict lncRNA-miRNA interactions, *Interdiscip. Sci*., **13** (2021), 535–545. https://doi.org/10.1007/s12539-021-00458-z
58. K. J. Chu, Y. S. Ma, X. H. Jiang, T. M. Wu, Z. J. Wu, Z. Z. Li, et al., Whole-transcriptome sequencing identifies key differentially expressed mRNAs, miRNAs, lncRNAs, and circRNAs associated with CHOL, *Mol. Ther. Nucleic Acids*, **21** (2020), 592–603. https://doi.org/10.1016/j.omtn.2020.06.025
59. L. Moreno-García, T. López-Royo, A. C. Calvo, J. M. Toivonen, M. de la Torre, L. Moreno-Martínez, et al., Competing endogenous RNA networks as biomarkers in neurodegenerative diseases, *Int. J. Mol. Sci*., **21** (2020), 9582. https://doi.org/10.3390/ijms21249582

AIMS Press